

Measurement of Thrust and Lift Forces Associated With Drag of Compliant Flapping Wing for Micro Air Vehicles Using a New Test Stand Design

D. Mueller · H.A. Bruck · S.K. Gupta

Received: 15 May 2008 / Accepted: 23 June 2009 / Published online: 10 July 2009
© Society for Experimental Mechanics 2009

Abstract Compliant wing designs have the potential of improving flapping wing Micro-Air Vehicles (MAVs). Designing compliant wings requires a detailed understanding of the effect of compliance on the generation of thrust and lift forces. The low force and high-frequency measurements associated with these forces necessitated a new versatile test stand design that uses a 250 g load cell along with a rigid linear air bearing to minimize friction and the dynamic behavior of the test stand while isolating only the stationary thrust or lift force associated with drag generated by the wing. Moreover, this stand is relatively inexpensive and hence can be easily utilized by wing designers to optimize the wing compliance and shape. The frequency response of the wing is accurately resolved, along with wing compliance on the thrust and lift profiles. The effects of the thrust and lift force generated as a function of flapping frequency were also determined. A semi-empirical aerodynamic model of the thrust and lift generated by the flapping wing MAV on the new test stand was developed and used to evaluate the measurements. This model accounted for the drag force and the effects of the wing compliance. There was good correlation between the model predictions and experimental measurements. Also, the increase in average thrust due to increased wing compliance was experimentally quantified for the first time using the new test stand. Thus, our measurements for the first time reveal the detrimental influence of excessive compliance on drag forces during high frequency operation. In addition, we were also able to observe the useful effect of compliance on the generation of extra thrust at the

beginning and end of upstrokes and downstrokes of the flapping motion.

Keywords Compliant flapping wing design · Thrust measurement · Lift measurement · Aerodynamic model · MAV

Introduction

There is now great interest in developing Micro-Air Vehicles (MAVs) that are very small with both fixed and flapping wing designs [1]. As the size of these MAVs decrease, the amount of thrust and lift that can be generated by the wing will also decrease, limiting the weight and payload capacity of the MAV. For very small MAVs with fixed wing designs, this will require critical air velocities that limit the maneuverability of the MAV. Thus, flapping wing designs can be more desirable, enabling the MAV to fly at air velocities approaching 0 (i.e., hovering), much like a rotorcraft structure. However, the flapping motion associated with these wing designs can produce thrust and lift forces that are more unsteady than fixed wing MAVs, which requires new measurement techniques for assessing the transient characteristics of these forces as a function of the flapping wing design.

Several researchers have developed mechanisms to realize the flapping motion and used these mechanisms in MAVs to demonstrate that these mechanisms can be used to achieve flapping wing flight. In this section we briefly review representative designs. Madangopal et al developed a flapping wing mechanism inspired by insect and bird flight [2, 3]. They presented the kinematic model and the rigid-body dynamics model of the mechanism and proposed an aerodynamic model of the wings' motion. Galinski and

D. Mueller · H.A. Bruck (✉, SEM member) · S.K. Gupta
Department of Mechanical Engineering, University of Maryland,
College Park, MD 20742, USA
e-mail: bruck@eng.umd.edu

Zbikowski examined the material challenges in the design of a wing in a flapping wing mechanism based on the insect hovering kinematics [4]. They concentrated on building a robust test rig design rather than a lightweight mechanism optimized for flight. Cox et al describe piezo-electrically actuated flexure-based skeletal mechanisms and wings for the electromechanical emulation of mesoscale flapping flight [5]. They developed and tested four-bar and five-bar mechanism designs. Banala and Agrawal developed a compound mechanism consisting of a five-bar and a four-bar mechanisms to mimic an insect wing motion [6]. Conn et al presented a biomimetic analysis of an insect flight and proposed biomimetic guidelines for mechanism simplification [7]. A novel parallel crank-rocker MAV flapping mechanism was chosen to replicate insect wing kinematics. Zdunich et al developed and tested the Mentor flapping wing MAV [8]. They described the experimental development of the wing design and its unsteady-airfoil analysis. They described two successfully flying prototypes and analyzed the flight tests results. Wood et al have worked on implementing gliding concepts inspired by insects on the centimeter scale [9]. Pronsin-sirirak et al have also looked at new materials, such as titanium alloys, for MEMS-based and non MEMS-based wings which were demonstrated on a palm-sized flapping wing MAV [10]. Michelson has also worked on implementing flapping wings in a multimode flying/crawling insect known as an “Entomopter”. [11].

There are numerous factors associated with the physical properties of air (e.g., density, viscosity) the physical characteristics of the wing (e.g., compliance, geometry), the flapping motion (e.g., frequency of flapping, degrees of freedom), and the forward motion of the flapping wing (e.g., Reynolds number, Strouhal number) that can affect lift and thrust. For a given flapping wing design, since the lift and thrust are coupled, these factors can simultaneously affect these forces. As a simple example, the higher the air density and the frequency of the flapping motion, the greater the lift and thrust. However, if the flapping motion becomes too vigorous, the compliance of a wing or air turbulence can cause instabilities that reduce lift and thrust. The level of lift and thrust that is capable of being generated by the flapping wing at a given flapping frequency will affect the amount of payload that the object can carry. Therefore, it is necessary to assess the dependence of the lift and thrust on wing shape and area in order to design a MAV that generates maximum thrust and lift with a minimum amount of weight [12, 13].

Measurement of lift and drag forces generated by MAVs have been obtained using traditional test stands, such as Able Corporation MKII [12]. However, they have been specifically designed for measuring forces of fixed wing MAVs in wind tunnels. Measurement of lift and drag in flapping wings has been accomplished using force trans-

ducers directly attached to the wing, such as the one used for Dickinson’s Robofly [13]. However, not all flapping wing designs are suitable for direct application of force transducers. Alternatively, a flapping wing MAV has been attached to a cantilever with a strain gage to obtain lift measurements [14], however the measurements are highly dependent on the materials properties and geometry of the cantilever and the cantilever design must be properly calibrated. It is also difficult to decouple the lift and thrust from the dynamic response of the cantilever beam to improve accuracy, so only the average thrust and lift is typically used.

Compliant wing designs are crucial for the functioning of flapping wing MAVs. During the flapping of the wings, the primary and secondary spars will deform to change the camber as well as the mid-chord velocities to influence lift and thrust forces during a flapping cycle. Existing computational and analytical models do not fully account for the effect of wing compliance on these forces, hence they are not adequate for designing and optimizing compliant wings. In addition, average thrust measurements are not adequate for fully characterizing the interaction between compliant wings and air. Hence, we need to perform dynamic thrust measurements to understand how thrust and lift forces are affected by the wing compliance during a flapping cycle. Dynamic thrust measurements will be useful for both optimizing the wing design and developing more detailed computational models for predicting thrust and lift. Hamamoto et al have previously conducted a numerical investigation into the effects of wing compliance [15].

In this paper, a new versatile test stand for measuring the thrust and lift of a flapping wing MAV is presented. The transient measurement capabilities of this test stand are investigated using a compliant flapping wing designed for a MAV weighing less than 15 g. Variation of the thrust and lift forces with flapping frequency and wing compliance are also investigated to demonstrate the ability of the test stand to assess the performance characteristics of a given compliant flapping wing design. The measured thrust and lift forces are compared with predictions from a semi-empirical aerodynamic model of the compliant flapping wing that accounts for drag forces and the compliance of the wing.

Compliant Flapping Wing MAV

A compliant flapping wing MAV has been developed in the Advanced Manufacturing Laboratory at the University of Maryland that weighs less than 15 g, illustrated in Fig. 1, using a novel drive mechanism and compliant wing design [16]. This MAV is capable of sustained flight with controlled ascent and descent both indoors and outdoors

Fig. 1 A flapping wing Micro-Air Vehicle (MAV) with a total weight of 13.2 g and details of the flapping wing mechanism

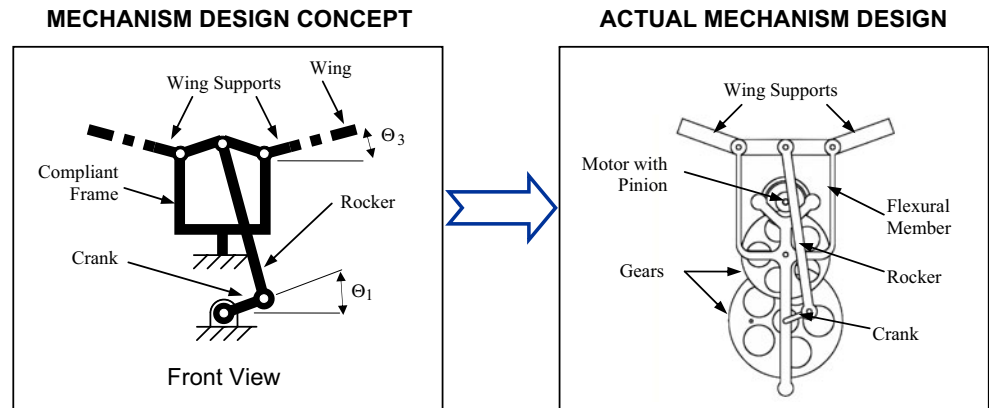
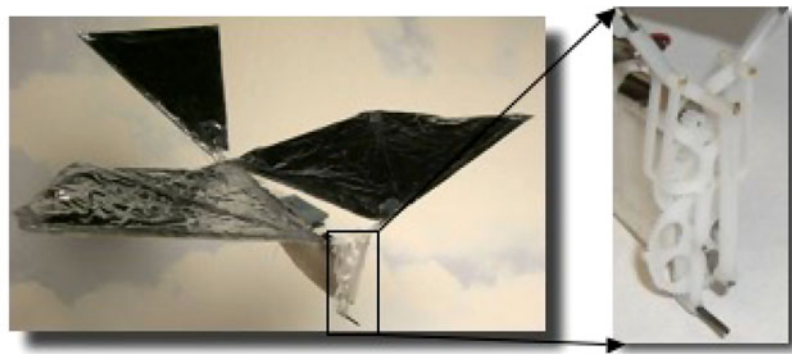


(Fig. 2). The main performance specifications for which the MAV has been designed are listed in Table 1.

For the version used in this paper, we machined the drive mechanism from Delrin plastic using 3-axis CNC machining. The wing was constructed using Mylar sheet and carbon fiber rods. The wing had one primary spar that formed the leading edge (Fig. 3). Increasing the diameter of the primary spar reduces compliance and increases weight. In addition, the wing had secondary spars to control the compliance of the wing with respect to the primary spar. The number of these spars can be increased to reduce

compliance. Wing designs with two different levels of compliance can be seen in Fig. 3, one rigid and one more compliant. The effect of this reinforcement on compliance can be seen in Fig. 4 where the displacement of the mid-chord for the semi-span of the wing is shown as a function of a point load applied using an Instron load frame and measured with a 250 g load cell. In this figure, it can be seen that there is a linear region corresponding to the localized stiffness of the wing where the rigid wing has about twice the localized stiffness of the more compliant wing. However, after about 1 mm, the more rigid wing

Fig. 2 Successful flight of the flapping wing MAV in Fig. 1

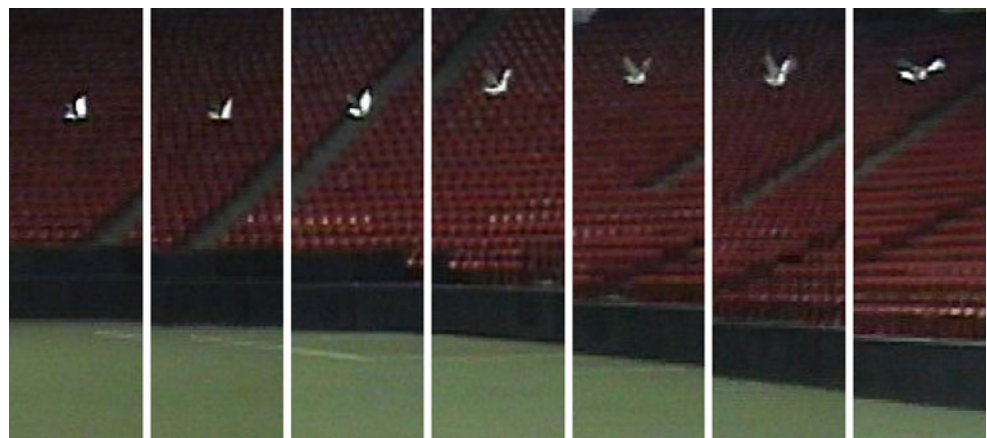


Table 1 Performance characteristics for the design of the flapping wing MAV in Fig. 1

| | |
|----------------------------|---------|
| Overall weight | 13.2 g |
| Maximum payload capability | 2.5 g |
| Maximum flapping frequency | 7.2 Hz |
| Flight duration | 5 min |
| Maximum flight velocity | 4.4 m/s |

shows a transition to a greater stiffness indicative of the compliance limit for the localized stiffness and transition to a global stiffness. This transition occurs at 3.5 mm for the more compliant wing, and the global stiffness is also approximately half that of the rigid wing. The overall effect is up to four times more deformation for the more compliant wing at the higher loading levels that will be associated with the measurements of the associated drag forces. The main effects of these two sources of compliance on the forces generated during flapping are described in Table 2. Wing compliance plays a crucial role in improving the performance. Excessive compliance will decrease stability and limit the force that the wing can sustain during flight. Too little compliance and the wing will be unable to change its camber to provide adequate thrust. Hence wing compliance need to be selected carefully. Unfortunately, current flapping wing models do not account for the effect of wing compliance on the force being exerted on the wing due to significant deformation of the wing during the flapping motion. Hence, the test stand described in this paper allows us to gain unique insight into the role of the wing compliance on thrust and lift forces. In particular, the

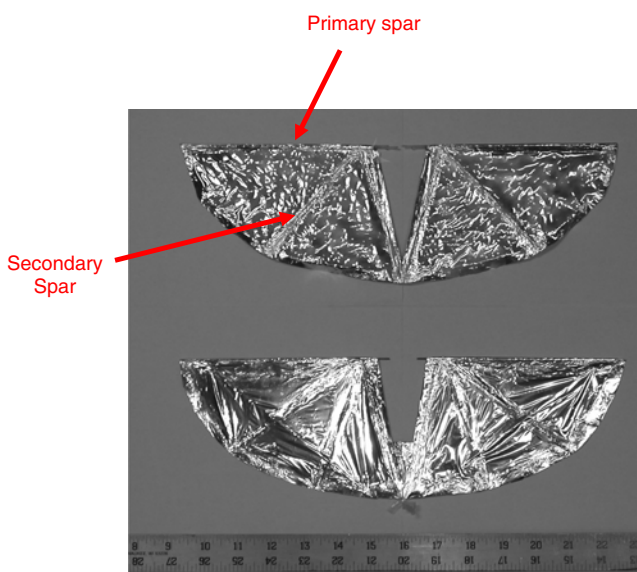


Fig. 3 Rigid wing (*bottom*) and compliant wing (*top*)

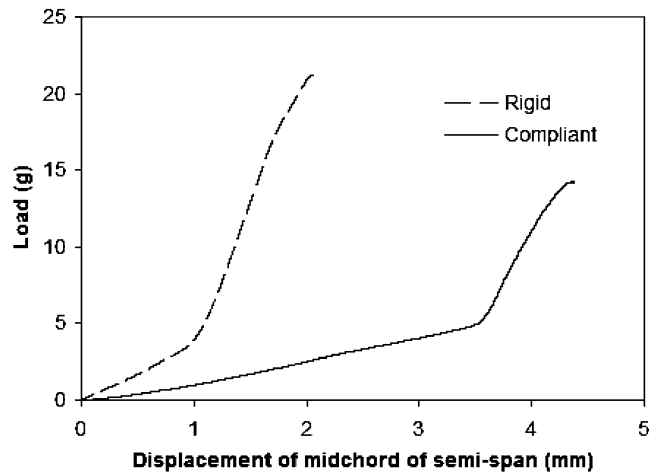


Fig. 4 A comparison of the compliance of the rigid and more compliant wing

effect of the wing compliance on these forces in response to the drag of the wing through the air (i.e., the drag forces) can be easily assessed.

New Test Stand for Thrust and Lift Measurement

In the absence of accurate computational models, designers of compliant wings will need to rely on the measurement of wing forces to understand the effects of different design parameters on the thrust and lift force profiles that will be generated during the flapping motion. To understand the tradeoff in these forces associated with compliance, it is sufficient to just characterize the force profiles generated by the drag of the wing without forward velocity. In order to make such a measurement device accessible and affordable, our goal was to develop the simplest possible test stand design that allows a user to perform dynamic measurement

Table 2 Source of compliance for the wing design and the main effects on aerodynamic forces

| Source of compliance | Main effects on aerodynamic forces |
|--|--|
| <i>Compliance of the primary spar</i> | <ol style="list-style-type: none"> 1. Controls stability at high frequencies. 2. Changes the projected wing area along flapping axis and perpendicular to the flapping axis. 3. Changes the effective velocity of the mid chord points of the wing. |
| <i>Compliance of the wing with respect to the primary spar</i> | <ol style="list-style-type: none"> 1. Allows the effective camber to reverse during the flapping cycle. 2. Changes the effective velocity of the mid chord points of the wing. |

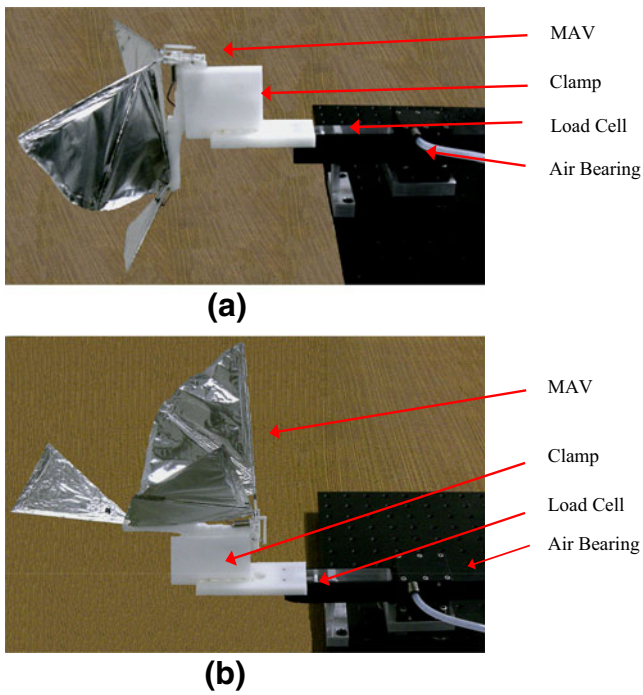


Fig. 5 The new test stand designed to measure thrust and lift of flapping wing MAVs

of wing forces due to drag with adequate accuracy. This test stand can be seen in Fig. 5. The primary component of this test stand is a rigid linear air bearing RAB1S from Nelson Air (Milford, NH) that has a steel slider bar 25.4 mm by 25.4 mm square in cross-section with a length of 150 mm to restrict motion to 1 DOF in order to isolate the thrust and lift forces that the wing generated. The friction in this linear air bearing is less than 0.1 g. The MAV is mounted in a clamp fixed to the end of the linear air bearing. A cavity was machined into the slider bar in order to mount a LFS270 load cell from Cooper Instruments (Warrenton, VA) with a 250 g capacity and 0.025 g resolution capable of measuring compressive loads generated by the flapping motion of the MAV. A Cooper Instruments DCM465 Bridge Amplifier was used to amplify the voltage, which was acquired with a National Instruments (NI) PXI-6040E cardbus data acquisition system using the NI Measurement & Automation Explorer software to record voltage as a function of time.

The test stand was placed on a vibration isolation stage in order to minimize the influence of vibrational forces on the measurements. Also, it was necessary to detach the MAV and turn it from the horizontal to vertical orientation with the mechanism facing up and tail facing down in order to measure lift. Flapping wings attached to a stationary platform are expected to produce close to zero average lift and a positive average thrust depending on the symmetry of the wing kinematics. The positive average thrust propels the flapping wing MAV forward and maintains the forward

velocity. The air traveling over the flapping wings generates the positive lift during the flight and keeps the flapping MAV airborne.

To validate the transducer response, an eccentric mass consisting of a 4.6 g steel rod 5 mm in diameter was placed 5 mm from the center of a motor. The motor was then rotated up to 1200 RPM to determine the response. The resulting measurements and comparison with the theoretical predictions can be seen in Fig. 6. The excellent correlation between the experimental results and theoretical predictions indicated that the system was capable of measuring flapping frequencies up to 20 Hz.

Semi-Empirical Aerodynamic Model for Flapping Wing

In order to understand the lift and thrust measurements from the new test stand, it is desirable to compare the experimental data with model predictions. Current flapping wing models, such as in reference [2] and in [17], do not take into account the changes in shape in the wing that occur at the apex and nadir of the flapping motion due to the compliance of the wing. This complex motion captures a significant amount of air that adds additional thrust to the thrust profile.

For the test stand measurements, thrust and lift forces are approximated by the drag of the wing through the air, which are modeled from reference [17] as follows:

$$\begin{aligned}
 L &= \int f_D \cos(\theta) dA = \int C_D \rho v^2 \cos(\theta) dA \\
 &= \int C_D \rho f^2 \cos(\theta) g^2(\theta_1) \cos(\theta_3) r^2 dA \\
 T &= \int f_D \sin(\theta) dA = \int C_D \rho f^2 \sin(\theta) g^2(\theta_1) r^2 dA
 \end{aligned}
 \tag{1}$$

where f_D is the drag force, C_D is the drag coefficient due to the shape of the wing that varies slightly with Reynold's number, ρ is the density of air, v is the wing velocity, f is the flapping frequency in Hz, ϑ is the standard camber angle determined by the shape of the wing, ϑ_1 is the rotation angle of the crank mechanism that determines the

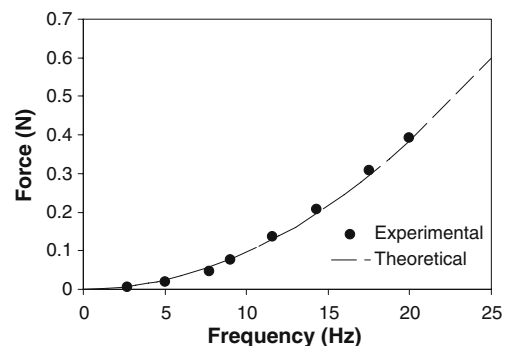


Fig. 6 The experimental and theoretical frequency response from the new test stand determined using a rotating eccentric mass

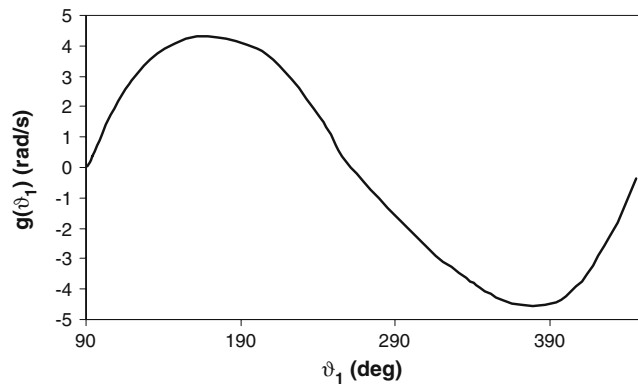


Fig. 7 Variation in the angular velocity of the wing versus the crank angle

wing velocity, ϑ_3 is the angle the primary spar makes with the horizontal plane during the flapping motion, r is the radial distance from the pivot point of the wing, and g is a function of ϑ_1 that relates the rotation angle of the crank mechanism to the angular velocity of the wing determined from the lengths of the shafts and the angles for the flapping mechanism. The relationship between the angles ϑ_1 and ϑ_3 in equation (1) is calculated using a kinematic analysis of the crank mechanism (the angles are illustrated on the crank mechanism in Fig. 1). Since the crank mechanism rotates at constant velocity, the cycle will be directly related to the position of the crank mechanism. A plot of $g(\theta_1)$ versus the angular position of the crank can be seen in Fig. 7.

The compliance of the wing has the possibility of further modifying thrust if it is at the proper level. For example, in the absence of compliance the level of thrust is simply controlled by the camber. Therefore, increasing compliance will enhance the level of thrust, however too much compliance will introduce instabilities during the flapping motion and completely eliminate thrust. To account for increasing thrust due to compliance, it is approximated as a change in the integrated thrust and lift on the wing in equation (1). The thrust and lift are only affected when the wing is at the nadir or apex, and the magnitude of the increase is proportional to the frequency. The constant of proportionality, k , was found to be 0.2, and varies as a single sine wave when the wing is 5 degrees before to 15 degrees after the apex or nadir is reached as determined from high speed video. The change in total drag force, ΔF_d , can be expressed empirically in terms of the angle of the crank shaft during the transition as follows:

$$\Delta F_d = (kf) \sin(\pi(\vartheta_1 - \vartheta_{1,begin}) / (\vartheta_{1,end} - \vartheta_{1,begin})) \quad (2)$$

where k is the constant of proportionality given in units of force-sec, and the angles of the crank shaft at the beginning and end correspond to the previously stated range of angles for the wing during the transition at the apex and nadir.

Note that the term contains the integrated effects of the wing area, so it is added directly to the thrust and lift force calculations in equation (1) and does not depend on the square of the frequency.

At higher frequencies, the larger drag forces cause more deformation of the wing due to compliance, which was quantified in Fig. 4. Thus, the results indicate the need for more complex computational fluid dynamics (CFD) analysis of the aeroelastic behavior of the compliant flapping wing structure to predict the coupling of the aerodynamic force and wing deformation. In lieu of a CFD analysis, the aerodynamic model was modified to approximately include the effects of compliance above 5 Hz that is evident in the bending of the primary spar in the plane perpendicular to the flapping axis. The compliance effects are also evident in Fig. 4 where there is a transition from local stiffness (i.e., deformation of internal spars) to global stiffness (i.e., deformation of edge spars) occurring at ~ 5 g (10 g for the whole MAV). The modification of the drag force was implemented by a reduction in the velocity in equation (1) above the transition point as follows:

$$v = (1 - [D_f / (c\delta)])v_o \quad (3)$$

where D_f is the level of the drag force above the transition point, c is the global stiffness of the wing determined above the transition point in Fig. 4, δ is the displacement of the midchord of the semi-span of the wing if it were infinitely rigid, and v_o is the velocity if it were infinitely rigid. Thus, the values used in equation (3) were experimentally determined using the measurements in Fig. 4. A summary of the experimentally determined and fit constants in equations (1) through (3) can be seen in Table 3.

Results and Discussions

Thrust measurements for the model flapping wing MAV obtained with the new test stand are shown in Fig. 8(a) for frequencies ranging from 3 to a maximum of 7.2 Hz. In particular, it can be seen that the average thrust is 0.077 N, with an amplitude of 0.011 Newton at the maximum

Table 3 Summary of constants used to calculate lift and thrust in equations (1) through (3) and how they are determined

| Constant | Determined by |
|---|--------------------------------|
| k (constant of proportionality) | Fit to thrust and lift data |
| ρ (density) | Known reference values |
| c (wing compliance) | Wing compliance measurements |
| C_D (drag force coefficient) | Wing shape and Reynolds number |
| δ (deflection of mid-chord of semi-span) | Wing compliance measurements |

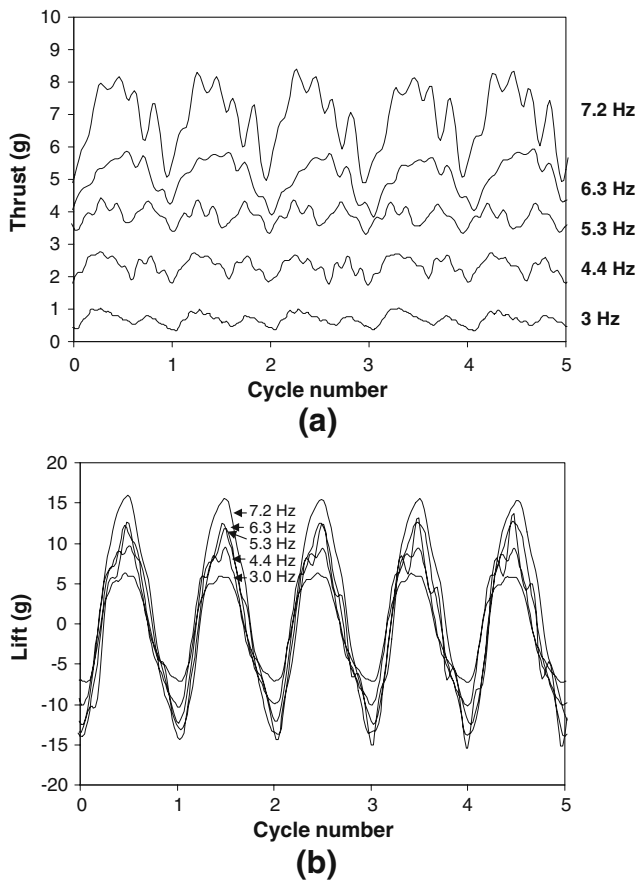


Fig. 8 Variation of (a) thrust and (b) lift profile with flapping frequency

frequency. The oscillations in the thrust are consistent with the flapping motion of the wings. In order to quantify the flapping frequency, a Fast Fourier Transformation (FFT) was applied to the data in Fig. 8 and the power spectrum shown in Fig. 9(a). The peak clearly corresponds to the flapping frequency of 7.2 Hz, but it is also clear that there are multiple peaks in the 33.5 Hz range. Dynamic loading tests conducted on the test stand without the MAV indicated that this frequency is due to the dynamic response of the test stand and is easily deconvolved via the FFT.

As the frequency decreases, it can be seen that the thrust decreases. Also, at higher frequencies, there appears to be a single peak during a cycle. However, as the frequency decreases below approximately 5 Hz, this single peak becomes a double peak. This thrust profile is characteristic of a change in camber due to the compliance of the wing, consistent with the profiles predicted for flapping wing MAVs [2, 13]. The effects of the flapping frequency on the average thrust and thrust amplitude can also be seen in Fig. 10(a). While the average thrust appears to increase with flapping frequency from 0.7 at 3 Hz to 7.7 g at 7.2 Hz, as would be anticipated from the basic behavior of flapping motion, the amplitude appears to vary only slightly from

0.6 at 3 Hz to 1.2 g at 7.2 Hz. This is also anticipated since the compliance of the wing does not vary with the flapping motion, therefore the amplitude is controlled by the camber.

After measuring the thrust, the MAV was detached and mounted 90° from horizontal to vertical. The variation in the lift profile versus frequency is shown in Fig. 8(b). At 7.2 Hz, the measured amplitude for the lift was 0.15 Newton. It also appears to be more sinusoidal than the thrust profile, which is expected since it is dominated by the flapping motion. Once again, the FFT power spectrum for the lift measurements, seen in Fig. 9(b), clearly indicates the peak at the flapping frequency of 7.2 Hz. However, unlike the thrust measurements, there is not a substantial peak at 33.5 Hz due to the dynamic response of the test stand. Fig. 8(b) indicates that these effects do not alter the lift profile as substantially as the thrust profile, since the amplitude of the lift is an order of magnitude greater than the thrust. The variation in amplitude and average lift with frequency is seen in Fig. 10(b). Once again, the amplitude of lift is increasing from 7.2 g at 3 Hz to 14.5 g at 7.2 Hz, however the average lift appears to vary insignificantly

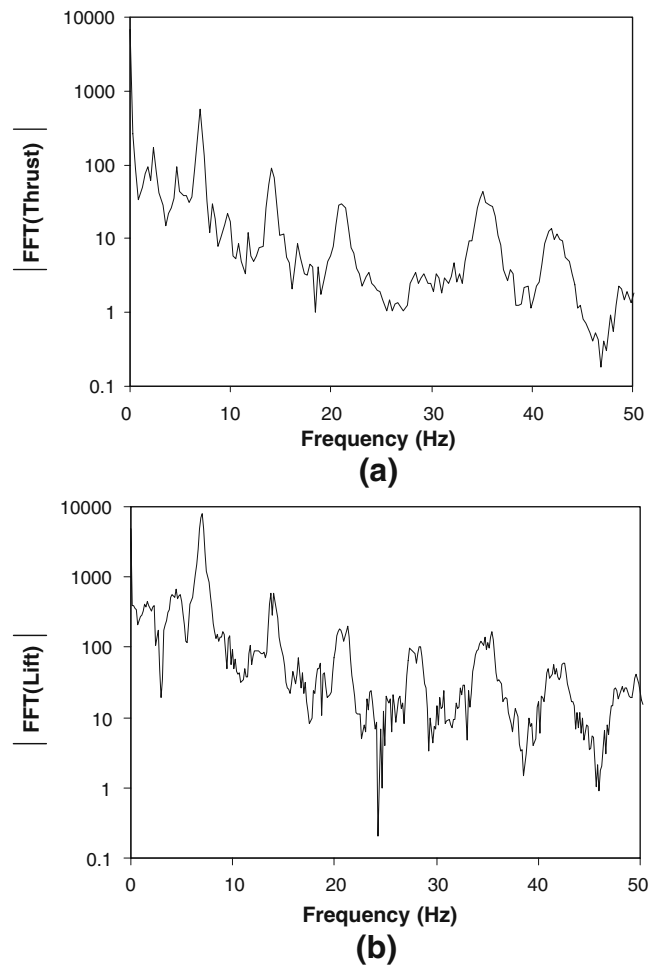


Fig. 9 FFT for (a) thrust and (b) lift measurements in Fig. 8

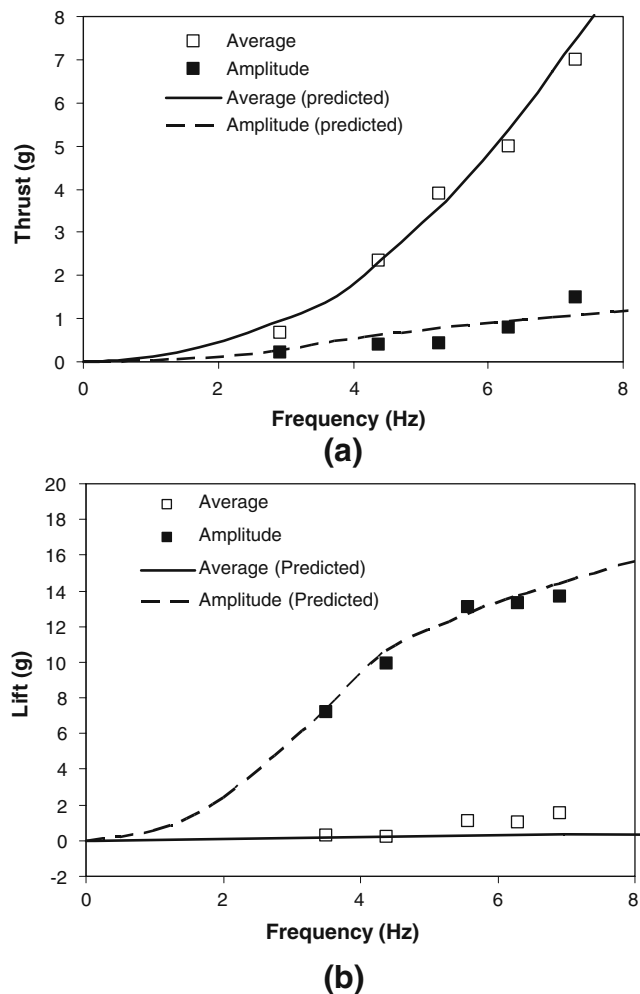


Fig. 10 Variation of (a) thrust and (b) lift force with flapping frequency and predictions from the model incorporating drag force and compliance of the wing

from 0.2 g at 3 hz to only 0.3 g at 7.2 Hz. Thus, the effect of flapping frequency on lift is opposite that of flapping frequency with thrust, which is to be expected from previous flapping wing models [2, 17].

Bending of the primary spar perpendicular to the flapping axis associated with the shape change due to compliance can easily be seen at higher frequencies using a high speed digital camera seen in Fig. 11. It appears that as the wing approaches the apex or nadir of the flapping motion, the primary spar bends backwards as the wing rotates towards the middle of the flapping motion. This bending causes a large change in the shape of the wing that encompasses a large volume of air that significantly changes the level of thrust due to compliance as frequency increases.

Comparisons of model predictions for the frequency variation of the measured amplitude and average values in thrust and lift can also be seen in Figs. 10(a) and (b). The drag coefficient C_D used in the model was 0.5, which is

fairly typical for these wing designs when the Reynolds number is above 1000. The experimental measurements correlate reasonably well with the model predictions, although the values of the lift are significantly lower at higher frequencies. More detailed comparison of the measured cyclic thrust and lift profiles at the lowest flapping frequency with the model predictions can be seen in Fig. 12, and correlate reasonably well since the flapping motion at this frequency is very stable. High speed images of the flapping motion at the maximum frequency of 7.2 Hz and the lowest frequency of 3.0 Hz in Fig. 13 indicate that compliance reduces the range of motion from -18 to 55 degrees at the lowest frequency to -10 to 45 degrees at the maximum frequency for a total loss of 20 degrees. This effectively translates to a loss of approximately 25% in velocity and a reduction in the resulting drag force of 40%.

Tests were also conducted on the more rigid wing design seen in Fig. 3. The thrust measurements can be seen in Fig. 14(a) and the lift measurements in Fig. 14(b). The

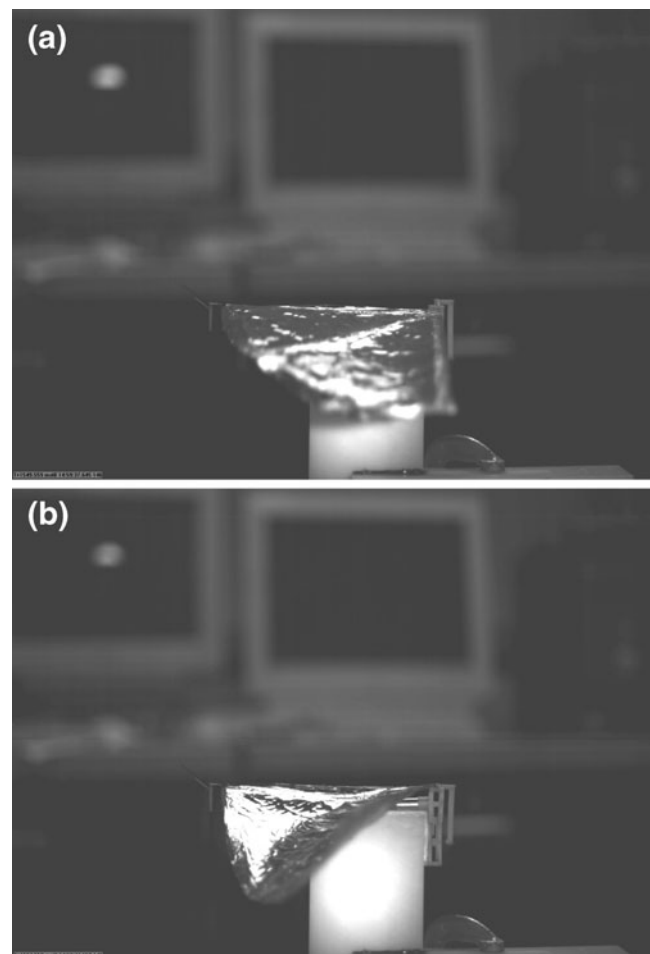


Fig. 11 Bending of the primary spar perpendicular to the flapping axis obtained using a high speed camera: (a) at the nadir, and (b) near the middle of the flapping motion

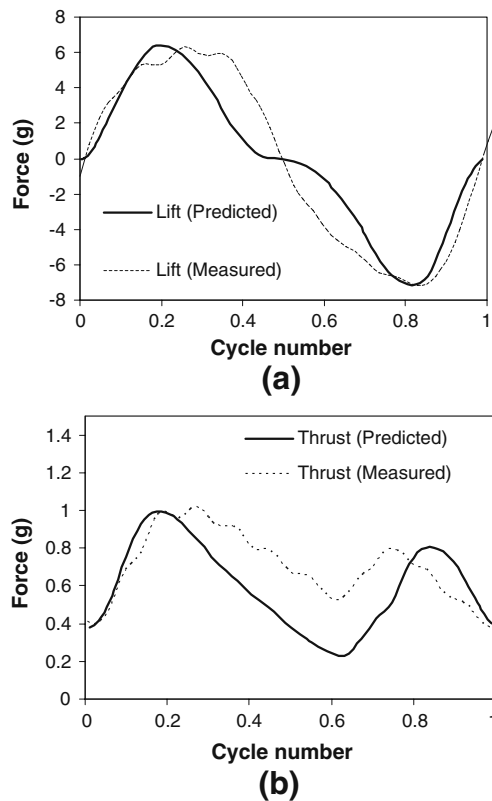


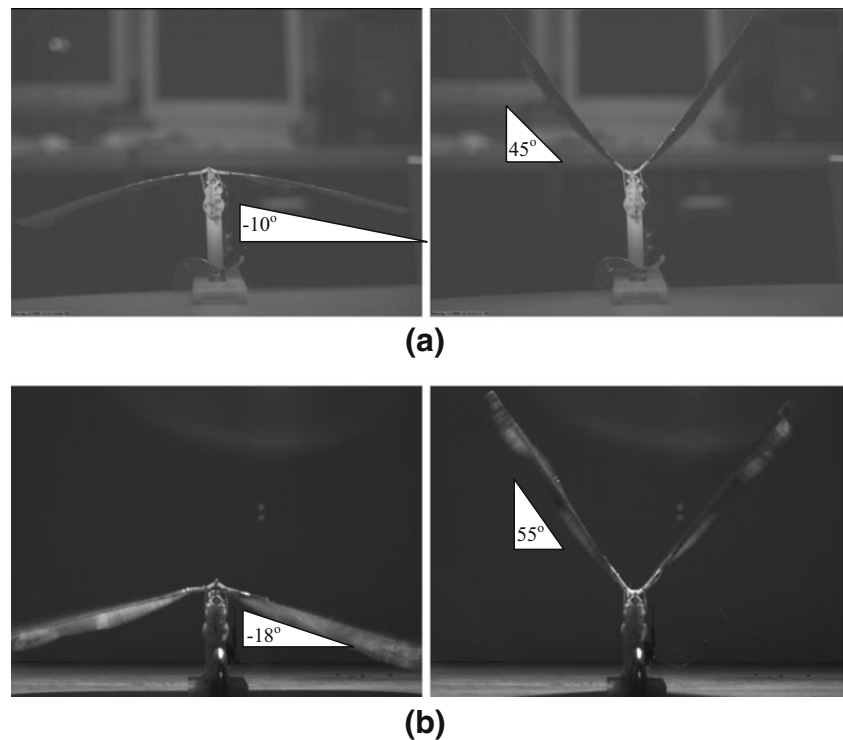
Fig. 12 Comparison of measured cyclic profiles for (a) lift and (b) thrust at minimum flapping frequency of 3.0 Hz with predictions from the model incorporating drag force and the compliance of the wing

resulting averages and amplitudes can be seen in Fig. 15. The effect of the additional reinforcement can be seen in the reduction of the level of thrust amplitude that is generated, and an increase in the lift of the wing. This is understandable given that the thrust amplitude is primarily due to the shape change that occurs at the apex and nadir of the flapping motion, and that the reduction in lift previously observed was due to compliance. With additional reinforcement, these shape changes are more constrained and the average thrust is subsequently reduced by approximately 1 g and the lift increases at higher frequencies. Thus, the effect of wing compliance has been experimentally quantified for the first time using the new test stand, and also correlates with the predictions from the aerodynamic model for the compliant flapping wing.

Conclusions

A new versatile test stand for measuring thrust and lift associated with drag forces generated by flapping wing MAVs is presented that minimizes frictional effects and the dynamic response due to the compliance of the test stand while isolating only a single component of the force generated by the flapping motion. The test stand is relatively inexpensive and hence can be easily utilized by the wing designers to optimize the wing compliance and

Fig. 13 High speed images of flapping motion at (a) 7.2 Hz and (b) 3.0 Hz showing change in the range of motion due to compliance of the wings at the higher frequency



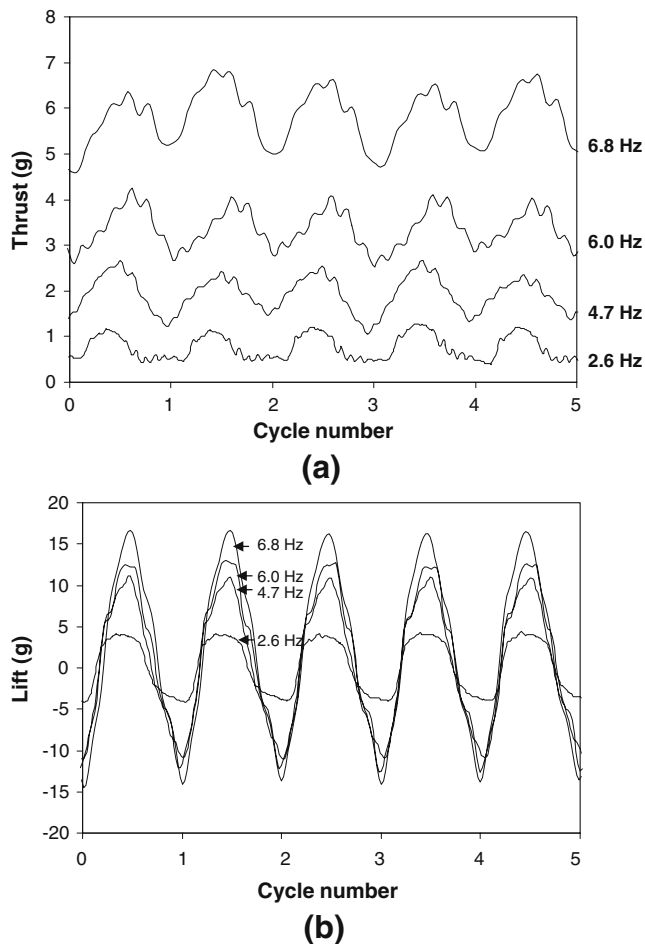


Fig. 14 (a) Thrust and (b) Lift measurements for wing modified to decrease compliance by adding more reinforcement

shape. It consists of a rigid linear air bearing with frictional forces below 0.1 g, and a load cell capable of measuring up to 250 g of force with 0.025 g of resolution. The test stand can easily accommodate any flapping wing MAV, and the load cell can be easily replaced to achieve even finer load resolution. A model flapping wing MAV structure has also been presented for characterizing the capabilities of the test stands in assessing the performance of a given flapping wing design.

The average value of the thrust force profile for the model flapping wing MAV was found to vary linearly from 0.7 at 3 Hz to 7.7 g at 7.2 Hz, while the amplitude appears to vary only slightly from 0.6 at 3 Hz to 1.2 g at 7.2 Hz. FFT analysis of the thrust force profile indicated dynamic effects from the load cell fixture at 33.5 Hz. These effects were less significant at lower frequencies, however bending effects from the compliance of the wing became clearly visible in the thrust profile.

Lift measurements indicated that the amplitude of lift is increasing approximately linearly from 7.2 g at 3 Hz to 14.5 g at 7.2 Hz, however the average lift appears to vary

insignificantly from 0.2 g at 3 Hz to only 0.3 g at 7.2 Hz. These trends were opposite those of the thrust measurements, but both are consistent with flapping wing models. FFT analysis of the lift force profile also indicated that the dynamic effects of the test stand at 33.6 Hz were far less significant since the amplitude was an order of magnitude greater than the thrust profile.

A semi-empirical aerodynamic model of the thrust and lift generated by the complex motion of the flapping wing MAV on the new test stand was used to analyze the measurements. This model accounted for drag force and compliance of the wing. There was good correlation between the model predictions and experimental measurements.

The effect of wing compliance was also experimentally quantified for the first time using the new test stand. By increasing the reinforcement on the wing, the shape changes that occur at the apex and nadir of the flapping motion were constrained resulting in a reduction in the average thrust of approximately 1 g. The variation in lift and drag with frequency also correlated well with the aerodynamic model of the compliant flapping wing. Thus, our measurements for the first time reveal the detrimental influence of excessive primary spar bending on the thrust and lift reduction under high frequency operation. In

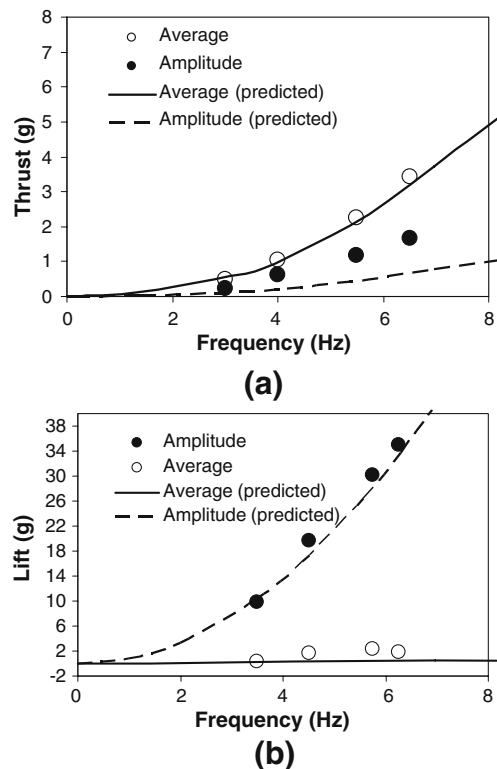


Fig. 15 Average and amplitude of (a) Thrust and (b) Lift measurements for more rigid wing design indicating a nearly perfect quadratic increase in lift amplitude with frequency and decrease in average thrust

addition, we are also able to observe the useful effect of compliance on the generation of extra thrust at the beginning and end of upstrokes and downstrokes of the flapping motion. We believe that the test stand reported in this paper can be used to obtain data to optimize the wing compliance as well develop detailed computational models for assessing the influence of wing compliance on thrust and lift.

Acknowledgements This research has been supported by the Army Research Office through MAV MURI Program (Grant No. ARMY W911NF0410176) and NSF grants DMI-0457058 and OCI-0636164. Opinions expressed in this paper are those of the authors and do not necessarily reflect opinions of the sponsors.

References

- Shyy W, Berg M, Ljungqvist D (1999) Flapping and flexible wings for biological and micro air vehicles. *Prog Aerosp Sci* 35:455–505
- Madangopal R, Khan ZA, Agrawal SK (2005) Biologically inspired design of small flapping wing air vehicles using four-bar mechanisms and quasi-steady aerodynamics. *J Mech Des* 127:809–816
- Madangopal R, Khan ZA, Agrawal SK (2006) Energetics-based design of small flapping-wing micro air vehicles. *IEEE/ASME Transactions on Mechatronics*, 11 (4)
- Galinski C, Zbikowski R (2007) Materials challenges in the design of an insect-like flapping wing mechanism based on a four-bar linkage. *Mater Des* 28(3):783–796
- Cox A, Monopoli D, Cveticanin D, Goldfarb M, Garcia E (2002) The development of elastodynamic components for piezoelectrically actuated flapping micro-air vehicles. *J Intell Mater Syst Struct* 13(9):611–615
- Banala SK, Agrawal SK (2005) Design and optimization of a mechanism for out-of-plane insect winglike motion with twist. *J Mech Des* 127(4):841–844
- Conn AT, Burgess SC, Ling CS (2007) Design of a parallel crank-rocker flapping mechanism for insect-inspired micro air vehicles. *Proc Inst Mech Eng, C J Mech Eng Sci* 221(10):1211–1222
- Zdunich P, Bilyk D, MacMaster M, Loewen D, DeLaurier J, Kornbluh R, Low T, Stanford S, Holeman D (2007) Development and testing of the mentor flapping-wing micro air vehicle. *J Aircr* 44(5):1701–1711
- Wood RJ, Avadhanula S, Steltz E, Seeman MM, Entwistle JJ, Bachrach A, Barrows G, Sanders S, Fearing RS (2007) An autonomous palm-sized gliding micro air vehicle—design, fabrication, and results of a fully integrated centimeter-scale MAV. *IEEE Robot Autom Mag* 14(2):82–91
- Pornsin-sirirak TN, Tai YC, Nassef H, Ho CM (2001) Titanium-alloy MEMS wing technology for a micro air vehicle application. *Sens Actuators A* 89(1–2):95–103
- Michelson RC (2004) Novel approaches to miniature flight platforms. *Proceedings of the Institution of Mechanical Engineers Part G-Journal of Aerospace Engineering*, 218(G5):363–373
- DeLuca AM, Reeder MF, Freeman J, Oi MV (2006) Flexible- and rigid-wing micro air vehicle: lift and drag comparison. *J Aircr* 43:2
- Sane SP, Dickinson MH (2002) The aerodynamic effects of wing rotation and a revised quasi-steady model of flapping flight. *J Biol* 205:1087–1096
- Muniappan A, Baskar V, Duriyanandhan V (2005) Lift and thrust characteristics of flapping wing Micro Air Vehicle (MAV). *AIAA-2005-1055*, 43rd AIAA Aerospace Sciences Meeting and Exhibit, Reno, Nevada, Jan. 10–13
- Mueller TJ (ed) (2001) “Fixed and Flapping Wing Aerodynamics for Micro Air Vehicle Applications,” AIAA Progress in Astronautics and Aeronautics, Vol. 195, Published by the American Institute of Aeronautics and Astronautics, Inc., Reston, VA
- Bejgerowski W, Ananthanarayanan A, Mueller D, Gupta SK (2009) Integrated product and process design for a flapping wing drive mechanism. *J Mech Des* 131:061006
- DeLaurier JD (1993) An aerodynamic model for flapping-wing flight. *Aeronaut J* 93:125–130